THESIS FOR THE DEGREE OF DOCTOR OF PHILOSOPHY

Statistical Analysis of Hardware Impairments in Communication Systems

Mohammad Hossein Moghaddam

CHALMERS
UNIVERSITY OF TECHNOLOGY

Department of Electrical Engineering
Chalmers University of Technology
Gothenburg, Sweden, 2023

Statistical Analysis of Hardware Impairments in Communication Systems

Mohammad Hossein Moghaddam
ISBN: 978-91-7905-968-2

Doktorsavhandlingar vid Chalmers tekniska högskola
Ny serie nr 5434
ISSN 0346-718X
This thesis has been prepared using LaTeX.

Department of Electrical Engineering
Chalmers University of Technology
SE-412 96 Gothenburg, Sweden
Phone: +46 (0)31 772 1000
`www.chalmers.se`

Printed by Chalmers Reproservice
Gothenburg, Sweden, 2023

To my family.

Abstract

This thesis delves into the study of hardware impairments, the inevitable limiting factors in radio frequency (RF) communication systems, and their substantial influence on system performance. It addresses the incongruity between the often stringent requirements imposed by standards and the innate imperfections of analog circuits present in real-world RF electronics. Key hardware impairments, namely In-phase and Quadrature-phase Imbalance (IQI), phase noise, power amplifier (PA) nonlinearities, and antenna array perturbations, are studied, offering comprehensive overviews of their individual characteristics and their interactions with each other.

The thesis also focuses on the effects of PA nonlinearity on widely used signal transmission optimizations, namely pulse shaping and matched filtering techniques. The nonlinear behavior of the PA, which can lead to signal distortions and inter-symbol interference, is shown to impact these techniques, posing considerable challenges to reliable communication. Moreover, a noticeable gap exists in the academic literature concerning an accurate analysis of the effect of PA nonlinearity on pulse shaping and matched filters. Such a gap underscores the need for a rigorous investigation into how these transmission optimizations are influenced by the PA's nonlinearity. As the first contribution of this thesis to the literature, in Paper A, a detailed study is conducted to comprehensively address these effects, bridging the existing knowledge gap and providing new insights into the interplay between PA nonlinearity, pulse shaping, and matched filter.

As a complementary study to Paper A, Paper B delves deeper into the intricacies of PA nonlinearity, examining the impact of various waveforms and modulation orders. Within this exploration, a waveform factor is formulated, elucidating the interplay between waveform statistics, amplifier-specific parameters, and signal power in determining the total distortion power. Furthermore, a theoretical closed form for the nonlinear distortion, both in-band and out-of-band, is derived. This derivation reveals a notable finding: the distortion approximately distributes evenly between the in-band and out-of-band portions of the spectrum, offering a nuanced understanding of how PA nonlinearity manifests across adjacent frequencies.

Moreover, in paper C, the effects of IQI and phase noise, in conjunction with PA nonlinearity, are analyzed, which can lead to a scrambled effect that further degrades the received signal quality. An additive noise modeling technique is

introduced as a novel approach to effectively represent these combined effects. This technique facilitates accurate tracking of system performance under varying hardware impairment conditions, serving as a valuable tool to understand the collective impact on the system and develop mitigation strategies.

The thesis further contributes to the field by providing statistical models for beam pattern variations due to antenna array perturbations in Paper D. The perturbations are random variations in phase, gain, and antenna element positions. These models enable an accurate projection of system performance under various conditions, helping to bridge the gap between theoretical design and practical implementation in RF communication systems.

This comprehensive investigation of hardware impairments in communication systems paves the way for more resilient design strategies, enhancing the robustness and reliability of future RF communication systems.

Keywords: Hardware impairments, PA nonlinearity, distortion analysis, pulse shaping and matched filter, phase noise, IQI, spectral analysis.

List of Publications

This thesis is based on the following publications:

[A] **M.H. Moghaddam**, S. Rezaei Aghdam, N. Mazzali, and T. Eriksson, "Statistical Modeling and Analysis of Power Amplifier Nonlinearities in Communication Systems". *IEEE Trans. comm.*, vol. 70, no. 2, pp. 822–835, Feb. 2022.

[B] **M. H. Moghaddam**, K. Buisman, and T. Eriksson, "Theoretical Analysis of Power Amplifier Distortion". Submitted to *IEEE Commun. Lett.*

[C] **M. H. Moghaddam**, S. Rezaei Aghdam, K. Buisman, and T. Eriksson, "Additive Noise Modeling: A Tractable Approach for Analyzing Residual RF Hardware Impairments". Submitted to *IEEE Trans. Veh. Technol.*

[D] **M. H. Moghaddam**, S. R. Aghdam, and T. Eriksson, "Statistical Analysis of Antenna Array Systems with Perturbations in Phase, Gain and Element Positions.". IEEE Global Conference on Signal and Information Processing, Ottawa, Ontario, Canada, Nov. 11-14, 2019.

Other publications by the author, not included in this thesis, are:

[E] **M. H. Moghaddam**, S. R. Aghdam, and T. Eriksson, "An Additive Noise Modeling Technique for Accurate Statistical Study of Residual RF Hardware Impairments". *2019 IEEE International Conference on Communications Workshops (ICC Workshops)*, Shanghai, China, May. 20-24, 2019.

[F] **M. H. Moghaddam**, S. R. Aghdam, A. Filippi, and T. Eriksson, "Statistical Study of Hardware Impairments Effect on mmWave 77 GHz FMCW Automotive Radar". *IEEE Radar Conference*, , Florence, Italy, Sep. 21-25, 2020.

Acknowledgments

As a PhD student nearing the completion of my journey at Chalmers, I wish to pause and extend my gratitude to those who provided the energy and motivation to persevere through this challenging endeavor, and to those I had the honor of collaborating with and learning from.

Foremost, I extend my most heartfelt thanks to my beloved family. Without their unwavering support and encouragement, I would not have reached this milestone. To my dear father, my closest friend and most profound teacher, your wisdom has shown me how to truly navigate life's path. To my beloved mother, your teachings of immense love and kindness are deeply cherished. Thank you for the unconditional love you have bestowed upon me. To my dear brother, my constant ally and pillar of support, I am profoundly grateful. And to my lovely sister, whose kindness and wisdom were always a comfort in times of need, thank you.

My deepest respect is for my supervisor, Professor Thomas Eriksson. I express my sincere gratitude for your guidance, encouragement, and counsel throughout these years. Working with you has been a blessing, and your kindness, as well as the memories of your incredible personality, will stay with me forever. I also extend my thanks to my co-supervisor, Dr. Sina Rezaei Aghdam, for our fruitful technical collaborations and the late-night weekend discussions, where your dedication to support me was invaluable.

I am grateful to Dr. Nicolo Mazzali for the very interesting discussions we had initially during a visit I had at ESA that later led to our joint collaborations in my research. My thanks also go to Prof. Koen Buisman for his support with the measurement setup I used in my research and for our collaborative efforts. I am thankful to Dr. Alessio Filippi and Marcel Geurts for hosting me at NXP Semiconductors during my research visit in the Netherlands. Additionally, my gratitude extends to Prof. Frans Willems for our enlightening discussions about mismatch decoders.

I also highly appreciate the understanding and patience of my current manager at Qamcom, Andreas Wolfgang, and my colleague Simon Lindberg for their support, which enabled me to finalize my PhD thesis while working at Qamcom.

I wish to acknowledge my special friend, Yasaman. The prospect of our friendship was a key motivator for me to come to Sweden and embark on this journey. Thank you for the cherished memories and for our continued friendship now. A big thank you also to my friends, Mohammad Ali Nazari (Manzar) and Kamran, for their assistance during my initial months in Sweden, and for their unwavering support over the years.

Last but not least, I thank all the seniors and colleagues at the department, including Professors, past and present COMSYS PhD students and Post-Docs, my office-mates Sven and Hao, and all our Silika project PhD fellows – Navid, Parastoo, Eduardo, Adrian, Artem, Marzieh, Tomislav, Corne, Ashkan, and Amr.

Sincerely,
Mohammad Hossein Moghaddam,
Göteborg, 2023

Acronyms

ACI:	Adjacent Channel Interference
ADC:	Analog-to-Digital Converter
AWGN:	Additive White Gaussian Noise
BB:	Baseband
BER:	Bit Error Rate
BS:	Base Station
CF:	Consumption Factor
CO2e:	Carbon Dioxide Equivalent
DAC:	Digital-to-Analog Converter
DPD:	Digital Pre-Distortion
GaN:	Gallium Nitride
GHG:	Greenhouse Gas
GSMA:	Global System for Mobile Communications Association
HWI:	Hardware Impairment
IBO:	Input Back-off
ICI:	Inter-Carrier Interference
IF:	Intermediate Frequency
i. i. d.:	independent and identically distributed
IMD:	Intermodulation Distortion
IQI:	In-phase and Quadrature Imbalance
ISI:	Inter-Symbol Interference

ITU:	International Telecommunication Union
LNA:	Low Noise Amplifier
LPF:	Low-Pass Filter
LO:	Local Oscillator
MAC:	Medium Access Control
MNO:	Mobile Network Operators
OFDM:	Orthogonal Frequency Division Multiplexing
PA:	Power Amplifier
PAPR:	Peak-to-Average Power Ratio
pdf:	Probability Distribution Function
PSN:	Phase Shifter Network
PN:	Phase Noise
QAM:	Quadrature Amplitude Modulation
QOS:	Quality of Service
RAN:	Radio Access Network
RF:	Radio Frequency
RRH:	Remote Radio Head
SDNR:	Signal-to-Distortion plus Noise Ratio
SISO:	Single-Input Single-Output
SNR:	signal-to-noise ratio
TRX:	Transceiver
UE:	User Equipment
VM:	Vector Modulator
VGA:	Variable Gain Amplifier

Contents

Part I

Overview

CHAPTER 1

Introduction

1.1 Background

In today's interconnected world, where seamless connectivity has become an essential part of our daily lives, the evolution of communication systems has played a pivotal role in transforming the way we connect, communicate, and share information. Among the most significant advancements in this field are cellular networks, which have witnessed remarkable progress over the years. As we stand at the precipice of the next technological frontier, it is crucial to examine the importance of connectivity and the role of new generations of cellular networks, such as 5G and the forthcoming 6G, in shaping the future of communication. Energy efficiency and hardware components are intrinsically linked when discussing the significance of connectivity and the role of new generations of cellular networks. These advanced networks are designed to handle massive data traffic and support a wide range of applications, including high-speed internet, augmented reality, autonomous vehicles, and smart cities. However, the increased computational demands and data processing requirements of these networks necessitate sophisticated hardware components capable of delivering high performance while minimizing energy consumption. Optimal hardware selection and design, such as power-efficient radio frequency (RF) chains, energy-saving transceivers, and intelligent antenna systems, is essential to enhance the energy efficiency of the network infrastructure. By effectively balancing the network's computational capabilities with power consumption, these hardware components contribute to the sustainability and long-term viability of the next technological frontier, ensuring that connectivity remains accessible and environmentally sustainable.

Energy Efficiency in Communication Systems

From 1937 to 2019, the global population experienced a significant growth, escalating from 2.3 to 7.7 billion individuals [1]. This population expansion, combined with the advent of modern agricultural practices, manufacturing advancements, transportation developments, and evolving lifestyles, has led to a substantial surge in energy consumption. Consequently, the atmospheric carbon concentration has risen from 280 to 409 parts per million during this time period [2]. Moreover, greenhouse gas (GHG) emissions have reached an unprecedented record of 37.5 gigatons of carbon dioxide equivalent (CO2e) in 2018, reflecting a 1.5% increase in comparison to the levels recorded in 2008 [3]. Governments and industries have thus undertaken, or are in the process of establishing, ambitious targets to mitigate GHG emissions and tackle the challenges posed by global warming [4], [5]. In this context, the enhancement of energy efficiency and reduction of energy consumption in communication networks play a pivotal role in curtailing GHG emissions. It is worth noting that beyond their direct impact, these networks hold the potential to act as enablers for addressing the prevailing climate change crisis, representing a crucial contribution by the mobile industry [6].

Notably, the advent of 5G communication capabilities has already had a profound impact on various sectors, including governments, existing industries, and emerging businesses. This impact stems from the improved effectiveness achieved through the utilization of resources in a more flexible, tailored, and efficient manner. To comprehend the scale and significance of this enabling effect of 5G, it is noteworthy to consider the estimations provided by the international telecommunication union (ITU) SMART 2020 report [7]. In 2018 alone, the enabling effect of mobile communications was assessed to be approximately 2,135 million tons of CO2e. Additionally, according to [8], this enabling effect is predicted to further escalate in the era of 5G, where the collective enabling effect across the entire information and communication technology sector is anticipated to account for 15% of global emissions by the conclusion of 2020. Furthermore, future projections indicate that the number of connected devices is expected to surge to 100 billion by 2030 [9]. Moreover, in terms of data capacity, 5G networks have demonstrated their potential to support a significantly larger volume of data compared to 4G networks, with estimates suggesting a capacity increase of up to 1,000 times that of 4G networks as observed in 2018 [10].

In order to accommodate the increasing demand for 5G (and in future for 6G) connectivity and fulfill its more stringent requirements, while simultaneously reducing energy consumption on a per-bit basis through intelligent network utilization, a paradigm shift is imperative. Mobile network operators (MNOs) must embrace novel approaches to network planning, deployment, management, and optimization that prioritize energy efficiency and encompass end-to-end implementation. Failing to prioritize energy efficiency in future 5G deployments, as highlighted in [11], could result in 5G networks consuming over 140% more energy than their 4G counterparts, despite the enhanced energy efficiency achieved in terms of bits per joule, owing to the larger bandwidth and superior spatial multiplexing capabilities of 5G. This undesirable energy consumption arises from the increased density of base stations (BSs), antennas, cloud infrastructure, user equipment (UE), and other factors associated with 5G networks. To address this challenge and gain insights into where meaningful energy reductions can be achieved within a 5G network, enabling MNOs to make informed decisions, the global system for mobile communications association (GSMA) conducted an insightful analysis [12]. This analysis highlights that the radio access network (RAN) constitutes the most power-intensive component, accounting for approximately 73% of the total power usage within a typical cellular network. This finding is corroborated by Vodafone's sustainability report in 2021 [13], which also demonstrates a 10% increase in RAN energy consumption over the past two years. Within a single BS, the radio frequency equipment, encompassing the power amplifier, transceivers, and cables, has been identified as the primary energy consumer, accounting for approximately 65% of the total BS energy [10], [14], [15]. The cooling system, digital signal and baseband processing, as well as the AC-DC converters, contribute to energy consumption levels of approximately 17.5%, 10%, and 7.5%, respectively. Consequently, contrary to the practices in 4G networks, the amount of always-on signaling in next-generation RANs must be substantially minimized. Of equal significance is the imperative to transmit and receive data, including the relevant signaling, to and from the designated UE, all while minimizing energy consumption to meet the quality of service (QoS) requirements of end-users [16]. It is crucial to prevent the wasting of resources through unregulated over-provisioning of end-users' QoS, as this plays a pivotal role in attaining substantial reductions in GHG emissions originating from RANs.

Base Station Power Consumption Breakdown

A BS consists of multiple transceivers (TRXs), with each TRX dedicated to serving several transmit antenna elements. Each TRX comprises several essential components, including a power amplifier, a radio frequency small-signal TRX module, a baseband part encompassing a receiver (uplink) and transmitter (downlink) section, a DC-DC power supply, an active cooling system, and an AC-DC unit (mains supply) for connection to the electrical power grid [17]. In the following, a brief explanation of the different components within the TRX is presented.

Antenna interface: The power efficiency of the communication system is influenced by the characteristics of the antenna, which can be represented by a set of losses. These losses include feeder losses, antenna bandpass filters, duplexers, and matching components. In the case of macro BS sites, which are often located separately from the antennas, an additional feeder loss of approximately -3 dB needs to be considered and accounted for [17]. To mitigate this feeder loss in macro BS setups, a remote radio head (RRH) can be implemented, where the power amplifier is installed at the same physical location as the transmit antenna. Conversely, feeder losses for smaller BS types are typically insignificant and can be neglected.

Power amplifier: Typically, the operational point that yields the highest efficiency for a power amplifier is in proximity to the maximum output power, nearing saturation. However, in practice, due to the presence of nonlinear effects and the utilization of Orthogonal Frequency-Division Multiplexing (OFDM) modulation with non-constant envelope signals, the PA is compelled to operate in a more linear region, typically 6-12 dB below saturation [17]. This operational approach is necessary to mitigate adjacent channel interference (ACI) caused by nonlinear distortions and thereby prevent performance degradation at the receiver. Nevertheless, this high operating back-off level leads to diminished power efficiency of the PA.

RF transceiver: The small-signal RF transceiver is comprised of separate receiver and transmitter components that facilitate uplink and downlink communication. The linearity and blocking specifications of the RF module can vary significantly based on the type of BS, thereby influencing the selection of the RF architecture [17]. Parameters that exert the most significant impact on RF energy consumption, denoted as PRF, include the required bandwidth, the allowable signal-to-distortion plus noise ratio (SDNR), and the resolution of the analog-to-digital conversion process.

Baseband unit: The baseband (BB) unit, responsible for digital signal processing, performs various operations such as digital up/downconversion, filtering modulation/demodulation, and digital pre-distortion [17]. It also handles signal detection tasks including synchronization, channel estimation, equalization, and compensation of RF non-idealities. Additionally, the BB engine encompasses channel coding/decoding processes. In the case of large BSs, the digital BB also accounts for the power consumption of the serial link connecting to the backbone network. Furthermore, the platform control and medium access control (MAC) operations contribute to the overall power consumption as they involve the control processor.

Power supply and cooling system: Power supply and cooling mechanisms play a vital role in the overall power consumption of communication systems. The losses associated with the DC-DC power supply, mains supply, and active cooling are directly proportional to the power consumption of the other components. It is important to note that active cooling is relevant only for macro BSs and is not applicable to smaller BS types[17]. Additionally, in the case of RRHs, active cooling becomes unnecessary as the PA is naturally cooled through air circulation.

Hardware Impairments in Communication Systems

As explained in the previous sections, the power efficiency of communication systems is a critical factor in achieving optimal performance. Hardware impairments, which encompass various imperfections and limitations in the components and subsystems of communication systems, have a profound impact on both power efficiency and spectral efficiency. Understanding these impairments is crucial for effectively optimizing power consumption and spectral efficiency in communication systems. By comprehensively studying hardware impairments, we can unlock valuable insights that enable us to design and deploy more energy-efficient and spectrally efficient communication systems.

As advancements in radio frequency electronic components technology continue to push the boundaries of their operational capabilities, the inherent imperfections of these components increasingly impact the performance of communication systems. However, there is a growing expectation to achieve higher spectral efficiency while utilizing low-cost electronic components in order to meet the ever-expanding demand for wireless access. To achieve a steady increase in spectral efficiency in the presence of hardware impairments, it becomes necessary to not only approach the physical limits defined by the Shannon bound but also to approach the engineering Shannon bounds that are determined by the technological limitations imposed by non-ideal hardware front-ends [18].

To approach the engineering bound we need to have a reliable model of hardware impairments. For doing so, we need to know the contribution of each hardware impairment effect on the system performance and the resulting cost for compensation in detailed scales [19]. In this way, accurate statistical modelings become very appealing for studying hardware impairments.

Hardware impairments modeling has been extensively studied in the literature [18], [20]. Some of the most important hardware impairments in communication systems are PA nonlinearity, phase noise in oscillators, and IQ imbalance in the modulator or demodulator. For many of these effects, dedicated algorithms have been developed to (partly) counteract the problems, such as digital pre-distortion (DPD) to invert a nonlinear amplifier [21], phase and frequency tracking algorithms to reduce the effects of phase noise and frequency offset [22], [23], algorithms to handle IQ imbalance [24], etc. However, even with such algorithms, there will be some residual distortions unaccounted for, due to e.g., parameter estimation errors and model mismatches that need to be studied accurately for hardware impairments (HWI) modeling.

1.2 Organization of the Thesis

This thesis is outlined in two parts. The first part includes two chapters, where we talk about the communications system fundamentals and hardware impairments in communication systems. The second part comprises four papers whose contributions were summarized in the abstract. The rest of the first part is organized as follows.

- In Chapter 2, we give a review of communication systems transceiver components.
- In Chapter 3, we explain the details of the most important hardware impairments and the way they can be formulated in system-level analysis. The main goal of Chapter 3 is to give an overall picture of the hardware impairments and to show how and in which subsystem of a communication system they can occur.
- In Chapter 4, we give a summary of the appended papers.

1.3 Notation

The following notation is used in the introduction. Superscript $(\cdot)^*$ denotes complex conjugate. For the first and second-order statistics, $\mathrm{E}[\cdot]$ and $\mathrm{Var}[\cdot]$ denote the expectation and Variance. for the complex random variables, $|(\cdot)|$, and $\angle(\cdot)$ denote the absolute value and phase of the complex random variables.

Vectors are denoted by boldface small letters, matrices are denoted by boldface capital letters, and the imaginary unit is represented by $j = \sqrt{-1}$.

CHAPTER 2

Communication Systems Transceiver Components

The field of digital communication systems is inherently intertwined with the architecture of transmitter and receivers, representing the cornerstone of information transmission and reception. Within this section, we undertake a granular inspection of different components of communication systems, dissecting their role, functionality, and interaction within the broader transceiver system. This analytical journey aims to facilitate a solid understanding of each component's function and how they interrelate within the larger transceiver framework. Our goal is not to delve into the exhaustive details of these components, but to present a coherent picture that enables the reader to understand their integral roles in the overall system. This fundamental comprehension paves the way for the following chapter, where we delve into the exploration of hardware impairments and their consequential effects on these critical components, casting light on the complex interplay between system architecture and its real-world performance limitations.

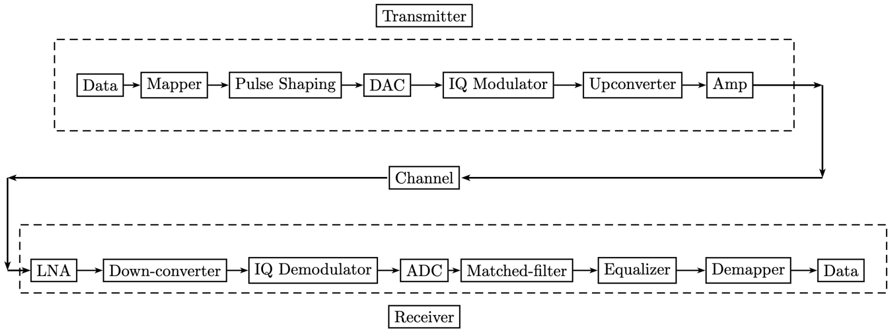

Figure 2.1: Transceiver Block Diagram

2.1 Transmitter

The transmitter is responsible for preparing the data for transmission over a physical medium. It consists of the following main components as depicted in Figure 2.1.

Data Source and Symbol Mapper

The data source provides the information to be transmitted, which often represented as a binary sequence

In digital communication, the symbol mapper maps the binary data into corresponding symbols that can be modulated and subsequently transmitted over the channel.

Focusing on M-QAM (Quadrature Amplitude Modulation), where M indicates the number of distinct symbols in the modulation scheme, the symbol mapper is responsible for converting $\log_2(M)$ bits into a single M-QAM symbol. The mapping operation adheres to a predefined mapping rule, typically guided by a constellation diagram, where each unique binary word is associated with a particular complex-valued symbol.

Mathematically, for a sequence of input bits $d_{n,k}$, where n represents the symbol index and k is the index of the bit within the symbol, the symbol mapper performs the following operation:

$$x_n = \mathcal{G}(d_{n,1}, d_{n,2}, ..., d_{n,\log_2(M)}) \tag{2.1}$$

Here, x_n denotes the n-th M-QAM symbol generated by the symbol mapper and $\mathcal{G}$ embodies the function executed by the symbol mapper to transform the binary input into an M-QAM symbol. The specific form of $\mathcal{G}$ varies depending on the constellation of the M-QAM scheme.

Pulse Shaping

Following the symbol mapping in the transmitter chain, the next critical stage is pulse shaping. The primary purpose of this operation is to shape each symbol into a waveform that is suitable for transmission over the physical channel. This is typically achieved using a pulse-shaping filter, which defines the temporal and spectral characteristics of the signal to be transmitted.

An important consideration in pulse shaping is to limit the bandwidth of the transmitted signal while minimizing inter-symbol interference (ISI). This balance is generally maintained through the careful design of the pulse-shaping filter. A widely used type of pulse shaping filter is the raised-cosine filter, characterized by its roll-off factor $0 \leq \beta < 1$ that determines the excess bandwidth beyond the Nyquist rate.

Given a sequence of symbols $x[n], n = 1, ..., N$ from the symbol mapper[1], the output of the pulse-shaping filter, $s[n]$, can be represented as:

$$s[n] = x[n] * g[n], \tag{2.2}$$

where $g[n], n = 1, ..., L$ is the impulse response of the pulse shaping filter. For a Raised-Cosine filter, the continuous-time $g(t)$ is given by:

$$g(t) = \frac{\sin(\pi t/T(1-\beta)) + 4\beta t/T \cos(\pi t/T(1+\beta))}{\pi t/T(1-(4\beta t/T)^2)}, \tag{2.3}$$

where T is the symbol period. When $\beta = 0$, this reduces to a sinc function, providing the minimum bandwidth for zero ISI, while for $0 < \beta < 1$, some excess bandwidth is allowed to control the time-domain characteristics of the signal.

The output $s[n]$ of the pulse shaping filter serves as the input to the subsequent stages in the transmitter chain, such as modulation and upconversion.

[1] here for simplicity we have considered pulse shaping for the complex digital baseband signal $x[n] = \Re[x[n]] + j\Im[x[n]]$.

Digital to Analog Converter (DAC)

Subsequent to the pulse shaping process in the transmitter chain, the digital signal is then forwarded to a Digital-to-Analog Converter (DAC). This unit serves a crucial function in the digital communication system, as it is responsible for converting the digital signal into an analog waveform that can be efficiently transmitted over the physical channel.

In a DAC, each digital sample is converted into an equivalent analog voltage level. The accuracy of this conversion is dictated by the DAC's resolution, which denotes the number of discrete analog levels the DAC can output. Higher resolution equates to a more faithful reproduction of the original analog signal.

For a band-limited input signal $s[n]$ that has been shaped into a digital signal, based on sampling theorem interpolation equation, the DAC can be mathematically represented as:

$$a(t) = \sum_{n=-\infty}^{\infty} s(n)\mathrm{sinc}(\frac{t - nT}{T}) \tag{2.4}$$

Here, $a(t)$ signifies the analog output of the DAC. The DAC's output for both the I and Q components of the signal are then separately forwarded to the IQ modulator for further processing.

IQ Modulator and Mixer

The output of the DAC in the transmitter chain, consisting of the separate I and Q components of the signal, is passed on to an IQ modulator.

Within the IQ modulator, the input signals are separately modulated onto cosine and sine carriers, both of which are 90 degrees out of phase with one another. Following the IQ modulation stage in the transmitter chain, the signal is upconverted to the carrier frequency using a mixer. Upconverter serves a fundamental role in preparing the signal for transmission over the air by shifting the frequency of the signal from baseband to a designated carrier frequency. The mathematical representation of the IQ modulator and mixer, which accepts the separate I and Q inputs, can be given by:

$$x(t) = I(t)\cos(2\pi f_c t) - Q(t)\sin(2\pi f_c t) \tag{2.5}$$

Here, $I(t)$ and $Q(t)$ represent the in-phase and quadrature components of the input signal $a(t)$, and f_c stands for the carrier frequency. The negative sign in the equation conforms to the convention that the quadrature component is 90 degrees behind the in-phase component.

After the signal has been upconverted, it is passed to the power amplifier, which increases the signal's power to a suitable level for transmission over the channel.

Power Amplifier

The power amplifier's primary role is to boost the signal power to a level suitable for effective transmission over the communication channel.

The power amplifier essentially multiplies the input signal by a constant gain, thereby increasing its amplitude. It's crucial to remember that this gain must be carefully selected to avoid driving the amplifier into non-linear regions, causing distortion and potentially creating out-of-band emissions that can interfere with other signals.

The operation of a power amplifier can be mathematically described by the equation:

$$p(t) = G_\mathrm{PA} y(t) \tag{2.6}$$

In this equation, $p(t)$ is the output signal of the power amplifier, G_PA is the gain of the amplifier, and $y(t)$ is the input signal from the upconverter.

This equation represents an ideal power amplifier that can perfectly amplify the signal without any distortion. However, in practical power amplifiers, the amplifier's non-linear characteristics and the possibility of gain compression need to be taken into consideration. These factors can lead to distortions in the amplified signal, necessitating the use of techniques such as DPD to compensate for these non-linearities.

Once the signal has been sufficiently amplified, it is ready to be transmitted over the communication channel.

2.2 Channel

In communication systems, channel is the physical medium over which the signal is transmitted. In wireless systems, this is the open air or space. A multitude of factors can influence the signal as it propagates through the channel, such as path loss, multipath propagation, shadowing, and Doppler shift.

Path loss results from the natural reduction in power density (attenuation) that occurs as a wireless signal propagates through space. Multipath propagation refers to the phenomenon where the wireless signals reach the receiver by multiple paths due to reflection, diffraction, and scattering. Shadowing is a signal fading effect, caused by obstructions such as buildings in the path of the signal. Doppler shift is the change in frequency (and hence the phase) of the signal due to the relative motion between the transmitter and the receiver.

However, for the purpose of our discussion, we will consider a simplified model known as the additive white Gaussian noise (AWGN) channel. In an AWGN channel, the only impairment is the linear addition of white noise to the transmitted signal. This is a common model for many digital communication links, especially those with a high signal-to-noise ratio (SNR).

The operation of the AWGN channel can be described by the equation:

$$r(t) = Ap(t) + n(t) \tag{2.7}$$

Here, $r(t)$ is the received signal, $p(t)$ is the transmitted signal after passing through the power amplifier, A is the attenuation factor mainly due to path loss, and $n(t)$ is the added white Gaussian noise. While the AWGN model is an oversimplification of real-world conditions, it provides an excellent starting point for understanding more complex channel models and effects.

2.3 Receiver

The receiver is responsible for recovering the original information from the received signal. The main components of the receiver are:

Low Noise Amplifier

At the beginning of the receiver's signal chain, the first component encountered is the low noise amplifier (LNA). As the received signal's power is typically very low due to path loss and other impairments, it needs to be amplified before further processing. The LNA's key role is to boost the signal's power while adding as little noise as possible, as any noise added at this stage would be amplified by subsequent components in the chain, thereby deteriorating the signal's quality.

The operation of the LNA can be mathematically described as follows:

$$s(t) = G_{\mathrm{LNA}} r(t) \tag{2.8}$$

In this equation, $s(t)$ represents the amplified signal, G_{LNA} is the gain of the LNA, and $r(t)$ is the input signal received from the channel.

The main challenge in the design of LNAs is the trade-off between gain, noise figure, and power consumption. The noise figure of an LNA is a measure of the degradation of the SNR caused by the LNA. The goal is to design an LNA with high gain, low noise figure, and low power consumption, but these three parameters are typically interrelated and cannot be optimized simultaneously.

After the signal has been amplified by the LNA, it is sent to the downconverter and IQ demodulator in the receiver chain for further processing.

Downconverter and IQ demodulator

Following the LNA, the amplified signal $s(t)$ is sent to the downconverter and IQ demodulator. The downconverter's task is to shift the frequency of the received signal from a high, possibly RF, frequency to baseband frequency for easier processing.

The operation of a downconverter and IQ demodulator is essentially a multiplication of the input signal with a local oscillator signal and its $\frac{\pi}{2}$ shifted version, to extract the in-phase (I) and quadrature (Q) components of the signal. These components carry the data encoded in the phase and amplitude of the transmitted signal:

$$I(t) = s(t)\cos(2\pi f_{\mathrm{c}} t) \tag{2.9}$$

$$Q(t) = s(t)\sin(2\pi f_{\mathrm{c}} t) \tag{2.10}$$

Here, $I(t)$ and $Q(t)$ are the in-phase and quadrature components of the signal respectively. Usually, the down-conversion and demodulation also include a low-pass filter to remove frequency components outside the bandwidth of the desired signal in the baseband.

These operations essentially correspond to projecting the signal onto the I and Q axes in the complex plane, which represent cosine and sine functions respectively. The result is a complex signal representation that fully captures both the amplitude and phase information of the original signal.

Following the demodulation, the I and Q components are sent to the ADC in the receiver's signal chain.

ADC

After demodulation, the analog I and Q components of the signal are converted into digital form using an Analog-to-Digital Converter (ADC). The ADC's task is to discretize the continuous-time, continuous-amplitude analog signal into a discrete-time, discrete-amplitude digital signal that can be processed by digital signal processing algorithms.

The conversion process performed by the ADC can be mathematically described as follows:

$$I[n] = \text{round}\left(\frac{I(t_n)}{\Delta}\right) \tag{2.11}$$

$$Q[n] = \text{round}\left(\frac{Q(t_n)}{\Delta}\right) \tag{2.12}$$

In these equations, $I[n]$ and $Q[n]$ represent the digital in-phase and quadrature components of the signal, respectively. $I(t_n)$ and $Q(t_n)$ represent the continuous-time in-phase and quadrature components of the signal at the sampling instants $t_n = nT_s$, where T_s is the sampling period. Δ is the quantization step size, which determines the resolution of the ADC, and the function round$(\cdot)$ rounds x to the nearest integer. Usually, a high-enough oversampling rate is considered in ADCs to fit the requirements for the matched filter as the next stage[2].

Following the ADC, the digital I and Q components of the signal are ready for further processing by the digital signal processing stages of the receiver.

Matched Filter

Following the ADC, the digital I and Q components of the signal, $I[n]$ and $Q[n]$, are sent to the matched-filter. The purpose of the matched-filter is to

[2] An oversampling rate of between 1.2-1.7 is usually enough for the matched filter according to indirect discussions we had with engineers at Ericsson

maximize the SNR at the detector input in the presence of AWGN. In other words, it is a filter whose impulse response is matched to the shape of the transmitted pulse, but reversed in time.

The operation of the matched-filter can be represented mathematically as follows:

$$I_f[n] = h[n] * I[n] \tag{2.13}$$

$$Q_f[n] = h[n] * Q[n] \tag{2.14}$$

In these equations, $I_f[n]$ and $Q_f[n]$ represent the filtered in-phase and quadrature components of the signal and $h[n]$ is the impulse response of the matched-filter.

After passing through the matched-filter, the filtered I and Q components are sent to the equalizer in the receiver's signal chain.

Equalizer

Once the signals have been processed by the matched-filter, the digital I and Q components of the signal, $I_f[n]$ and $Q_f[n]$, are then sent to the equalizer. An equalizer is employed to compensate for channel distortion such as multi-path interference and ISI that could alter the properties of the transmitted signal.

An equalizer essentially reverses the effect of channel, represented by the channel impulse response $h_{ch}[n]$. In the simplest form, for a linear equalizer, the operation can be represented mathematically as follows:

$$I_e[n] = g[n] * I_f[n] \tag{2.15}$$

$$Q_e[n] = g[n] * Q_f[n] \tag{2.16}$$

Here, $I_e[n]$ and $Q_e[n]$ represent the equalized in-phase and quadrature components of the signal and $g[n]$ is the impulse response of the equalizer. The impulse response $g[n]$ of the equalizer is chosen to be an approximation of the inverse of the channel impulse response $h_{ch}[n]$.

In reality, equalization is a complex problem and a perfect inversion of the channel is often not possible. Advanced equalization techniques such as adaptive equalization and decision feedback equalization are used in practice.

After passing through the equalizer, the equalized I and Q components are ready for further processing by the subsequent stages in the receiver's signal chain.

Symbol Demapper

Following equalization, the digital I and Q components of the signal, $I_e[n]$ and $Q_e[n]$, are then sent to the symbol demapper. The symbol demapper performs the inverse operation of the symbol mapper in the transmitter side. Specifically, it maps the received symbols back into bits.

In the case of M-QAM modulation, the mapping operation is determined by the constellation diagram, and the demapper can be implemented as a look-up table or decision algorithm that associates each received symbol with the closest valid M-QAM symbol.

Mathematically, for M-QAM, the symbol demapper performs the operation

$$\hat{d}[n] = \text{argmin}_{d \in \mathcal{D}} \sqrt{(I_e[n] - I_d)^2 + (Q_e[n] - Q_d)^2} \tag{2.17}$$

where $\mathcal{D}$ is the set of valid M-QAM symbols, each represented by a pair of in-phase and quadrature components (I_d, Q_d), and $\hat{d}[n]$ is the estimated bit or bit-group of the n-th symbol. The function argmin is used to find the symbol in $\mathcal{D}$ that is closest to the received symbol $(I_e[n], Q_e[n])$, in terms of the Euclidean distance in the IQ plane.

After symbol demapping, the estimated bits $\hat{d}[n]$ are output and form the final received bit stream in the communication system.

CHAPTER 3

Hardware Impairments in Communication Systems

This section is dedicated to exploring four critical hardware impairments that commonly affect communication systems: IQI, phase noise, PA nonlinearities, and antenna array perturbations. Each of these hardware imperfections can substantially affect the performance of communication systems, leading to signal degradation and, in turn, reduced system efficiency. Understanding their mechanisms, the mathematical modeling associated with each, and their collective impact on signal transmission is critical to optimizing system performance. These insights can also enhance our ability to navigate the challenges that arise from these impairments, enabling more effective system design and implementation. In the context of this study, the in-depth reviews of these impairments aim to equip readers with a solid foundation to facilitate the understanding of more complex analyses presented in the appended papers.

3.1 Modelling of hardware impairments

Accurate modeling of hardware impairments is essential to analyze and optimize the performance of communication systems. In this section, we discuss the importance of statistical modeling of hardware impairments.

Statistical modeling approaches can be done in two different ways. One explicitly accounts for treating hardware impairments as stochastic processes that evolve over time. The other approach focuses on the variability introduced during the manufacturing process considering the fact that no two hardware units are identical due to slight differences in manufacturing processes, material quality, and assembly practices. The primary difference between these two methods lies in their focus and application. In this thesis, the stochastic process approach is mainly discussed in Papers A-C, and the manufacturing process variability is mainly discussed in Paper D.

Overall, statistical modeling of hardware impairments in communication systems offers a practical and effective approach to understanding and managing the impact of non-ideal components.

In the literature, statistical models of hardware impairments mostly pertain to the statistical modeling of observations. They describe the aggregated effects of all residual hardware impairments using an i.i.d. additive Gaussian noise model [25]–[37]:

$$y(t) = h(x(t) + \eta_t(t)) + \eta_r(t) + w(t) \tag{3.1}$$

where h, η_t, η_r, and $w(t)$ represent the channel model, aggregated HWI effects on the transmitter side, aggregated HWI effects on the receiver side, and additive noise of the channel respectively. While this model offers a straightforward approach to analyzing residual hardware impairments, it lacks the accuracy required to capture the detailed parameters of scrambled residual hardware impairment effects.

In this thesis, and more specifically in Papers A-C, we follow a different approach. We examine the transceiver's output as stochastic processes rooted in true hardware models. Deriving stochastic processes from these true hardware models aids in understanding the critical parameters of various components within communication systems. In our approach, we intend to model HWI as a scaled useful signal part plus uncorrelated distortion where the distortion is modeled as a function of parameters of HWI. This approach effectively captures the impact of different hardware impairments, especially when the effects of specific impairments are pronounced. Recognizing the extent to which certain impairments overshadow others provides insights into hardware bottlenecks. Additionally, this understanding allows for enhanced model accuracy and optimization of the balance between design complexity (cost) and performance. Notably, it provides a term-by-term description of both individual and cumulative effects of hardware impairments. The extensive details of this model are discussed in the appended papers of this thesis.

In the following sections, we explain the hardware impairment effects in communication systems and provide statistical models for them according to our proposed approach.

3.2 IQI

In a communications system, the in-phase (I) and quadrature (Q) branches play a crucial role in determining the quality of the received signal. However, the lack of perfect matching between the I and Q branches in practical systems leads to hardware impairments commonly referred to as in-phase and quadrature imbalances (IQI). IQI results from imperfections in analog circuits, such as differences in the amplitude or phase of the I and Q components of the signal. These imbalances lead to signal degradation and can affect the system's performance considerably.

IQI Modeling in Communication Systems

At the heart of IQI is the non-ideal nature of the quadrature hybrid, the circuit element designed to create a $\frac{\pi}{2}$ phase difference between the I and Q signals. In an ideal world, the quadrature hybrid would have perfect $\frac{\pi}{2}$ phase difference and equal gain in both branches. However, in reality, mismatches in component values, non-idealities in active devices, and a host of other factors create an imbalance between the I and Q branches. These imbalances can be modeled as gain and phase errors in either the I or Q branch or both [20], [38]. Asymmetrical IQI models, where both phase and gain imbalances are considered in only one branch, have been shown to be equivalent to symmetrical IQI models for single-input single-output (SISO) systems [20]. The LOs at the transmitter side by considering asymmetric imbalance as illustrated in Figure 3.1 have the form of

$$\mathrm{LO_I} = \cos(2\pi f_c t), \tag{3.2}$$

$$\mathrm{LO_Q} = -g_{\mathrm{T}}\sin(2\pi f_c t + \psi_{\mathrm{T}}), \tag{3.3}$$

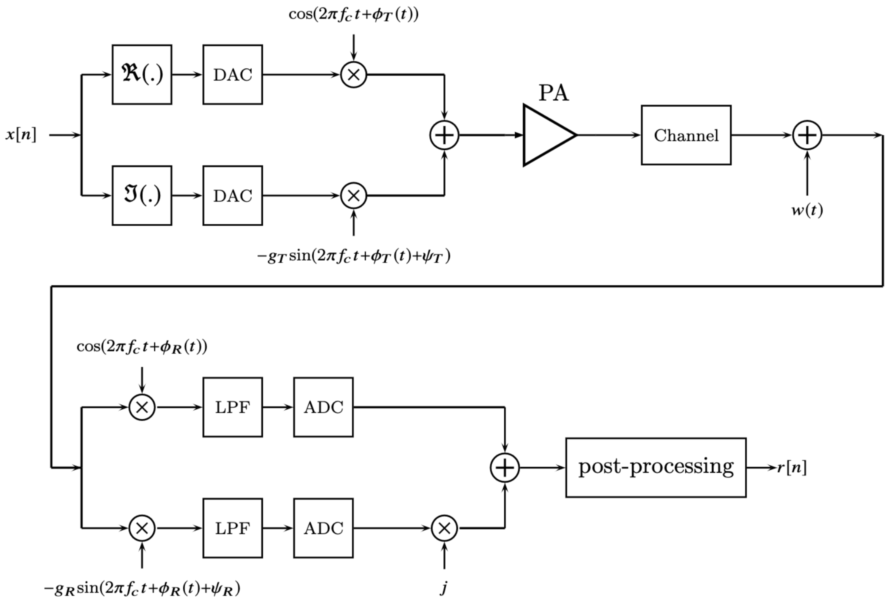

Figure 3.1: System model.

where g_{T} and ψ_{T}, are gain and phase imbalances due to IQI. The baseband signal x_k is divided into in-phase (x_{I}) and quadrature (x_{Q}) branches using a divider, and then transformed into analog signals using a DAC for each branch, as described by the following equations:

$$x_{\mathrm{I}}(t) = \sum_{k=-L}^{L} \Re[x_k]\mathrm{h}\,(t - kT), \tag{3.4}$$

$$x_{\mathrm{Q}}(t) = \sum_{k=-L}^{L} \Im[x_k]\mathrm{h}\,(t - kT), \tag{3.5}$$

where $\mathrm{h}(t)$ is the pulse-shaping filter with $2\mathrm{L}+1$ taps and T is the sampling rate. The RF signal after passing through the LOs according to (3.2) and

(3.3) is given by [20]:

$$
\begin{aligned}
x_{\mathrm{RF}} &= (\Re[x(t)]\cos(2\pi f_c t) - \Im[x(t)] g_{\mathrm{T}} \sin(2\pi f_c t + \psi_{\mathrm{T}})) \\
&= \frac{\left[\left(\Re[x(t)] + j g_{\mathrm{T}} e^{j\psi_{\mathrm{T}}} \Im[x(t)]\right) e^{j2\pi f_c t} + \left(\Re[x(t)] - j g_{\mathrm{T}} e^{-j\psi_{\mathrm{T}}} \Im[x(t)]\right) e^{-j2\pi f_c t}\right]}{2},
\end{aligned}
\tag{3.6}
$$

where, by defining α_{T} and β_{T}

$$
\alpha_{\mathrm{T}} = \frac{1 + g_{\mathrm{T}} e^{j\psi_{\mathrm{T}}}}{2}, \tag{3.7}
$$

$$
\beta_{\mathrm{T}} = \frac{1 - g_{\mathrm{T}} e^{j\psi_{\mathrm{T}}}}{2}, \tag{3.8}
$$

we can re-write (3.6) as

$$
x_{\mathrm{RF}}(t) = \frac{(\alpha_{\mathrm{T}} x(t) + \beta_{\mathrm{T}} x^*(t))\, e^{j2\pi f_c t} + (\alpha_{\mathrm{T}}^* x^*(t) + \beta_{\mathrm{T}}^* x(t))\, e^{-j2\pi f_c t}}{2}. \tag{3.9}
$$

Finally, the baseband equivalent of the RF signal affected by IQ imbalances is given by:

$$
x_{\mathrm{IQI}}(t) = \alpha_{\mathrm{T}} x(t) + \beta_{\mathrm{T}} x^*(t). \tag{3.10}
$$

In the case of symmetric IQI, (3.10) still holds but with α_{T} and β_{T} change to [39]:

$$
\alpha_{\mathrm{T}} = \cos(\psi_{\mathrm{T}}/2) + j g_{\mathrm{T}} \sin(\psi_{\mathrm{T}}/2), \tag{3.11}
$$

$$
\beta_{\mathrm{T}} = g_{\mathrm{T}} \cos(\psi_{\mathrm{T}}/2) - j \sin(\psi_{\mathrm{T}}/2). \tag{3.12}
$$

For the receiver LO in I and Q branches we have:

$$
\mathrm{LO_I} = \cos(2\pi f_c t), \tag{3.13}
$$

$$
\mathrm{LO_Q} = -g_{\mathrm{R}} \sin(2\pi f_c t + \psi_{\mathrm{R}}), \tag{3.14}
$$

and the received signal after the low-pass filter (LPF) will be

$$
\begin{aligned}
r(t) =& \mathrm{LPF}[\cos(2\pi f_c t) x_{\mathrm{RF}}(t)] + j\ \mathrm{LPF}[-g_{\mathrm{R}} \sin(2\pi f_c t + \psi_{\mathrm{R}}) x_{\mathrm{RF}}(t)] \\
&= \mathrm{LPF}\left[\Re[x_{\mathrm{RF}}(t) e^{j2\pi f_c t}] + j\Im[g_{\mathrm{R}} x_{\mathrm{RF}}(t) e^{-j(2\pi f_c t + \psi_R)}]\right],
\end{aligned}
\tag{3.15}
$$

where by defining α_R and β_R

$$\alpha_{\mathrm{R}} = \frac{1 + g_{\mathrm{R}} e^{-j\psi_{\mathrm{R}}}}{2}, \tag{3.16}$$

$$\beta_{\mathrm{R}} = \frac{1 - g_{\mathrm{R}} e^{j\psi_{\mathrm{R}}}}{2}, \tag{3.17}$$

the baseband received signal can be represented as

$$r(t) = \mathrm{LPF}\left[\alpha_{\mathrm{R}} x_{\mathrm{RF}}(t) e^{j2\pi f_c t} + \beta_{\mathrm{R}} x^*_{\mathrm{RF}}(t) e^{-j2\pi f_c t}\right]. \tag{3.18}$$

The effect of IQI can be compensated by pre-processing algorithms, but still, some residual effects remain that are referred to as residual IQI. For the residual IQI, normally, the phase and gain imbalances are very small.

Statistical Modeling of IQI

In statistical modeling, we intend to formulate the impaired signal as a useful signal plus uncorrelated distortion. In the processing chain of communication systems, and after IQI compensation, the residual IQI contains small values of $\beta_{\mathrm{T}}, \beta_{\mathrm{R}} \approx 0$ and $\alpha_{\mathrm{T}}, \alpha_{\mathrm{R}} \approx 1$. Considering these residual parameters, the second part in (3.18) can be modeled as distortion, uncorrelated with the first part. If we consider a zero-mean x_{RF}, then the distortion part can be modeled as a zero-mean random process whose variance is a function of β_{R} and variance of x_{RF}. In the aggregated statistical models [25]–[37], the total distortion is usually modeled as a Gaussian random process according to equation (3.1). In another approach, which is the focus of Paper C, we aim for a more accurate analysis of how residual IQI parameters can affect the final signal where we consider the hardware models into account. So, if we consider both transmitter and receiver IQI in an AWGN channel, the baseband equivalent of the received signal has the form of

$$r(t) = \underbrace{\left(\alpha_{\mathrm{R}}\alpha_{\mathrm{T}} + \beta_{\mathrm{R}}\beta^*_{\mathrm{T}}\right) x(t)}_{\text{useful signal}} + \underbrace{\left(\alpha_{\mathrm{R}}\beta_{\mathrm{T}} + \beta_{\mathrm{R}}\alpha^*_{\mathrm{T}}\right) x^*(t)}_{\text{distortion}} + \underbrace{\alpha_{\mathrm{R}} w(t) + \beta_{\mathrm{R}} w^*(t)}_{\text{noise}}, \tag{3.19}$$

where $w(t)$ is the additive white Gaussian noise of the channel. As we see the useful signal is scaled by IQI parameters, and the distortion part can be modeled as a stochastic process whose higher order statistics have the trace of IQI parameters from transmitter and receiver which, scrambled together with the complex conjugate of the signal of interest. Using (3.19), the signal impaired by IQI can be more accurately modeled according to the IQI parameters that are explained in detail beside other HWI effects in Paper C.

3.3 Phase noise

The presence of phase noise in the transmitter LO can significantly impact the performance of wireless communication systems, especially those operating at high frequencies or with low-cost hardware components. Phase noise in oscillators, which are used for up-conversion and down-conversion, is primarily caused by thermal noise in the oscillator circuitry. This results in fluctuations in the oscillator's phase that can cause errors in the transmitted and received signals, leading to lower signal quality [40]. At its root, phase noise is an outcome of the fact that an oscillator is never perfectly stable, and small, random deviations from the perfect oscillation frequency occur, creating a "jitter" in the phase of the signal.

Modeling of Phase Error in Communication Systems

The presence of phase error $\phi_{\mathrm{T}}(t)$ in the transmitter LO results in the following representation for the I and Q branches:

$$\mathrm{LO}_{\mathrm{I}} = \cos(2\pi f_c t + \phi_{\mathrm{T}}(t)), \tag{3.20}$$

$$\mathrm{LO}_{\mathrm{Q}} = -\sin(2\pi f_c t + \phi_{\mathrm{T}}(t)), \tag{3.21}$$

where the same oscillator source feeds both I and Q branches. The result of up-converting the baseband signal $x(t)$ is the RF signal x_{RF} given by

$$\begin{aligned} x_{\mathrm{RF}}(t) &= (\Re[x(t)]\cos(2\pi f_c t + \phi_{\mathrm{T}}(t)) - \Im[x(t)]\sin(2\pi f_c t + \phi_{\mathrm{T}}(t))) \\ &= \frac{x(t)e^{j(2\pi f_c t + \phi_{\mathrm{T}}(t))} + x^*(t)e^{-j(2\pi f_c t + \phi_{\mathrm{T}}(t))}}{2}. \end{aligned} \tag{3.22}$$

The $\phi_{\mathrm{T}}(t)$ is the discrepancy between the expected phase of the signal and its actual phase. Phase errors can occur due to various reasons, such as instability in the local oscillator, imperfections in the mixing process, or environmental factors affecting the signal path. The presence of phase error can corrupt the signal, leading to a loss of information. This is especially critical in systems that rely on precise phase information, like many digital modulation schemes.

Statistical Modeling of Residual Phase Noise in Communication Systems

When phase errors occur during upconversion or downconversion, they manifest as phase noise in the signal. It can be thought of as adding a kind of "jitter" to the signal's waveform.

The phase noise process $\phi_{\mathrm{T}}(t)$ in the transmitter's LO as in (3.22), and $\phi_{\mathrm{R}}(t)$ in the receiver's LO are assumed to be uncorrelated. They are usually modeled by a Wiener process whose variance increases linearly with time at an unknown rate c, so the variance of the phase noise is given by $\sigma_{\mathrm{T}}^2 = \mathrm{E}[\phi_{\mathrm{T}}^2(t)] = ct$ [20].

The effect of phase noise can be compensated using a phase tracker at the receiver side. However, there are always some residual errors that cannot be compensated, which are referred to as residual phase noise. The equivalent baseband form of the received signal in its simplified form with phase noise effects of transmitter and receiver before the phase tracker can be shown as

$$x_{\mathrm{PN}}(t) = x(t)e^{j\phi_{\mathrm{PN}}(t)}, \tag{3.23}$$

where $\phi_{\mathrm{PN}} = \phi_{\mathrm{T}}(t) + \phi_{\mathrm{R}}(t)$ is the combined effect of transmitter and receiver phase noise. In the phase tracker, most of the ϕ_{PN} is compensated, keeping the residual phase noise variance low, so

$$\Delta\phi(t) = \hat{\phi}(t) - \phi_{\mathrm{PN}}(t), \tag{3.24}$$

where $\hat{\phi}(t)$, and $\Delta\phi(t)$ are the estimated phase noise out of phase tracker, and residual phase noise. As a result, the residual phase noise is significantly reduced by the phase tracker, resulting in $\Delta\phi(t) \ll 1$.

For the statistical modeling of the residual phase noise, we usually model the residual phase noise $\Delta\phi$ as a zero-mean Gaussian random process. Depending on the level of accuracy, by using Taylor expansion, the exponential form of the phase noise can be decomposed to

$$e^{j\Delta\phi(t)} = 1 + j\Delta\phi - \frac{\Delta\phi^2}{2} - j\frac{\Delta\phi^3}{6} + ..., \tag{3.25}$$

where then (3.23) can be re-written as

$$x_{\mathrm{PN}}(t) = \gamma_{\mathrm{PN}} x(t) + d_{\mathrm{PN}}(t), \tag{3.26}$$

where the useful signal $\gamma_{\mathrm{PN}} x(t)$ is uncorrelated with distortion $d_{\mathrm{PN}}(t)$ and its gain γ_{PN} can be obtained as

$$\gamma_{\mathrm{PN}}(t) = \frac{\mathrm{E}\left[x_{\mathrm{PN}}(t)x^*(t)\right]}{\mathrm{E}[x(t)x^*(t)]} = \left(1 - \frac{\sigma_{\mathrm{PN}}^2}{2} + ...\right), \tag{3.27}$$

where we have used Bussgang decomposition [41]. Then by using (3.23),(3.26), and (3.27), $x_{\mathrm{PN}}(t)$ can be decomposed into useful and uncorrelated distortion signals as

$$\begin{aligned} x_{\mathrm{PN}}(t) &= x(t)(1 + j\Delta\phi - \frac{\Delta\phi^2}{2} - j\frac{\Delta\phi^3}{6} + ...) \\ &= \frac{\mathrm{E}\left[x_{\mathrm{PN}}(t)x^*(t)\right]}{\mathrm{E}[x(t)x^*(t)]} x(t) + d_{\mathrm{PN}}(t) \\ &= \underbrace{\left(1 - \frac{\sigma_{\mathrm{PN}}^2}{2} + ...\right) x(t)}_{\text{useful signal}} + \underbrace{\left(j\Delta\phi - j\frac{\Delta\phi^3}{6} + ... + \frac{\sigma_{\mathrm{PN}}^2}{2} - \frac{\Delta\phi^2}{2} + ...\right) x(t)}_{\text{distortion}}, \end{aligned} \tag{3.28}$$

where σ_{PN}^2 is the variance of the residual phase noise. In (3.28), the distortion part can be modeled as a stochastic process which has the trace of higher-order statistics of the phase noise. In Paper C, we study in detail how this statistical model can be beneficial in case of scrambled effects of other HWIs.

3.4 PA nonlinearity

The operation of a PA is intrinsically nonlinear when it is driven into its high-efficiency, near-saturation operating region. Such nonlinearity introduces amplitude and phase distortions to the transmitted signal, leading to spectral regrowth, which can infringe on adjacent frequency bands [42]–[44]. Furthermore, in multi-carrier systems like OFDM, PA nonlinearity exacerbates issues of intermodulation distortion (IMD) and inter-carrier interference (ICI), degrading the overall system's bit error rate (BER). Consequently, understanding and mitigating the implications of PA nonlinearity becomes paramount to upholding the integrity of communication systems. In the following section, we delve into the details of PA nonlinearity and modeling in communication systems.

Modeling of PA Nonlinearity in Communication Systems

To mathematically capture the nonlinear effects of PAs, mathematical tools such as Volterra series [45], [46] are employed.

Based on the Weierstrass theorem [47], every continuous function defined on a closed interval can be uniformly approximated by a polynomial function. Now, for the passband signal

$$x_{\mathrm{RF}}(t) = \Re[x(t)]\cos(2\pi f_c t) - \Im[x(t)]\sin(2\pi f_c t) = \frac{x(t)e^{j2\pi f_c} + x^*(t)e^{-j2\pi f_c}}{2}, \tag{3.29}$$

the output of the PA according to the Weierstrass theorem can be expressed as:

$$y_{\mathrm{RF}}(t) = g(x_{\mathrm{RF}}(t)) = a_0 + a_1 x_{\mathrm{RF}}(t) + a_2 x^2_{\mathrm{RF}\mathrm{RF}}(t) + a_3 x^3_{\mathrm{RF}}(t) + ..., \tag{3.30}$$

where a_is are the coefficients dependent on the specific characteristics of the PA [48]. This memoryless polynomial model represents the distortion caused by the PA in most case scenarios.

It is usually more convenient to represent (3.30) as a function of the complex baseband signal $x(t)$ as [49]

$$y(t) = \sum_{p=0}^{P} \gamma_{2p+1} x(t)|x(t)|^{2p}, \tag{3.31}$$

where $y(t)$ is the complex baseband equivalent of the PA output with γ_{2p+1} as the PA coefficients for the baseband equivalent form. Note that in (3.31) only odd-order terms are present since the signals generated by even-order terms are far from the carrier frequency and their effects are removed after applying passband filters [50].

In Paper A and Paper B, we show that for reasonable input back-offs (IBO), the third-order PA nonlinearity ($P = 1$) is sufficient to model most of the distortion. Figure 3.2 depicts the spectrum for different orders of PA nonlinearity for a Gallium Nitride (GaN) power amplifier, using the RF-Weblab [51]. It is observable that the third-order distortion is typically considerably more significant, surpassing other higher-order distortions by over 20 dB according to within the in-band region of the spectrum. It is a typical behavior for many amplifiers in the most practical range of IBO.

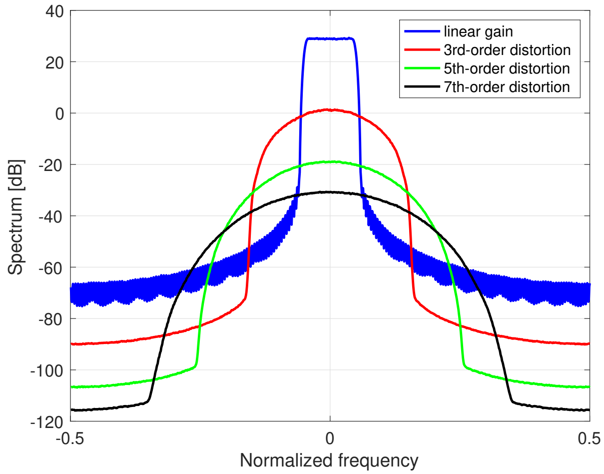

Figure 3.2: PA output linear gain together with higher-order distortions based on measurements for a Gallium Nitride (GaN) power amplifier, the Cree CGH40006-TB model [51] (Fig. 1 in Paper B).

Statistical Modeling of PA Nonlinearity in Communication Systems

Statistical models offer an alternative perspective, highlighting the probabilistic behavior of PA nonlinearity in real-world scenarios. Rooted in stochastic processes, these models are inherently flexible, often leading to analytical tractability, particularly in complex communication systems systems. Leveraging these models can be particularly beneficial for performance studies since they establish a direct connection between PA nonlinearity and key system metrics, including bit error rate, signal-to-distortion plus noise ratio (SDNR), and channel capacity.

To deliver the statistical modeling of PA nonlinearity in communication systems, we follow the definition in (3.31). The nonlinearity effect in (3.31) can be equivalently expressed through a statistical model as

$$y(t) = \gamma x(t) + d(t), \tag{3.32}$$

where $d(t)$ represents the distortion due to nonlinearity and is statistically uncorrelated with $x(t)$. The coefficient γ can be determined as [52]

$$\gamma = \frac{\mathrm{E}[y(t)x^*(t)]}{\mathrm{E}[x(t)x^*(t)]}. \tag{3.33}$$

In aggregated HWI modeling, as seen in [25]–[37], the distortion component $d(t)$ is typically modeled as a Gaussian random process. While this modeling can be apt for certain scenarios, it might not capture the detailed characteristics of PA nonlinearity in the final model.

As a different approach in Paper A, we delve into the modeling of PA nonlinearity in communication systems by focusing on third-order nonlinearity effects based on the model in (3.31) and the intricacies of the pulse shaping and matched filter. A similar approach was followed in the master thesis by Adrian Lahuerta [53], and the work in paper A can be seen as a continuation of that work. According to our model in Paper A and [53], the symbol-level received signal is expressed as

$$y_n = \gamma_1 x_n + w_n' + \underbrace{\gamma_3 \int_{-\infty}^{\infty} \sum_{k=-\infty}^{\infty} x_k h_{s-k} \left| \sum_{l=-\infty}^{\infty} x_l h_{s-l} \right|^2 h_{s-n}^* \, ds}_{d_n}\,. \tag{3.34}$$

with $h(\cdot)$ as the pulse shaping filter and d_n represents the distortion. Following (3.34), we construed the nonlinearity as a tripartite model, encompassing power scaling, constellation deformation, and amplifier-induced noise that comprises different moments of the input signal, reflecting the intricacies of pulse shaping and matched filtering:

$$y_n = \tilde{x}_n \underbrace{\left(\alpha_1 \sigma_x + \alpha_3 \sigma_x^3 \mu_1\right)}_{\text{scaling of power}} \underbrace{\left(1 + \frac{\alpha_3 \sigma_x^3 \mu_3 |\tilde{x}_n|^2}{\alpha_1 \sigma_x + \alpha_3 \sigma_x^3 \mu_1}\right)}_{\text{constellation deformation}}$$
$$+ \underbrace{\alpha_3 \sigma_x^3 \left(c_n^{(0)} + c_n^{\prime(1)} |\tilde{x}_n| + c_n^{(2)} |\tilde{x}_n|^2\right)}_{\text{amplifier}-\text{induced noise}} + \underbrace{w_n'}_{\text{AWGN}} . \tag{3.35}$$

This nuanced categorization in Paper A offers a more holistic view of PA nonlinearity. Additionally, Paper A carves out a unique niche by deriving the SDNR anchored in its detailed statistical model. Coupled with the analysis of IBO optimization and corroborated by extensive simulation-based observations, Paper A delineates the pragmatic relevance and broader utility of the model in (3.35).

For devising effective linearization strategies and optimizing system performance, it is beneficial to make statistical studies of PA nonlinearity at the transmitter side. In Paper B, by considering the inherent over-sampled signal at the transmitter side, we study both in-band and out-of-band distortion. We show that the PA nonlinearity at the transmitter side can be effectively modeled by the third-order polynomial model and that the resultant distortion power comprises three distinct parts, the variance of the input signal, the PA-specific nonlinearity parameter, and a waveform part that is a function of higher-order statistics of the input signal

$$\sigma_d^2 = \sigma_x^6 |\gamma_3|^2 \underbrace{\left(\frac{\mathrm{E}\left[|x(t)|^6\right]}{\sigma_x^6} - \frac{\left(\mathrm{E}\left[|x(t)|^4\right]\right)^2}{\sigma_x^8}\right)}_{\text{waveform-dependent part}} . \tag{3.36}$$

In paper B, we show how this model presents different properties based on different waveforms, pulse shaping filters, and which in some cases can make the distortion PDF deviate from Gaussian to other distributions. Our proposed waveform parameter bears a relationship to peak-to-average power ratio (PAPR), as it similarly penalizes high signal values via high-order moments (4th and 6th order). However, here we highlight the direct correlation between the proposed parameter and nonlinear distortion, which could render it particularly useful for evaluating waveforms.

3.5 Statistical modeling of the Combined Effects of IQI, PN, and PA nonlinearity in Communication systems

In case of combining the HWI effects together, there will be scrambled effects that make the modeling of hardware impairments more complicated. Combining the effects of IQI, PN, and PA nonlinearity, in Paper C, we show that the resultant complex form can be formulated as

$$
\begin{aligned}
y(t) =& A\alpha_{\mathrm{R}} \left(\sum_{p=0}^{\infty} \gamma_{2p+1} \sum_{k=0}^{p+1} \binom{p+1}{k} (\alpha_{\mathrm{T}} x(t))^{k} (\beta_{\mathrm{T}} x^{*}(t))^{p+1-k} \right. \\
& \sum_{k=0}^{p} \binom{p}{k} (\alpha_{\mathrm{T}}^{*} x^{*}(t))^{k} (\beta_{\mathrm{T}}^{*} x(t))^{p-k} e^{j\phi_{\mathrm{PN}}(t)} \\
& + A^{*}\beta_{\mathrm{R}} \left(\sum_{p=0}^{\infty} \gamma_{2p+1}^{*} \sum_{k=0}^{p} \binom{p}{k} (\alpha_{\mathrm{T}} x(t))^{k} (\beta_{\mathrm{T}} x^{*}(t))^{p-k} \right. \\
& \left. \sum_{k=0}^{p+1} \binom{p+1}{k} (\alpha_{\mathrm{T}}^{*} x^{*}(t))^{k} (\beta_{\mathrm{T}}^{*} x(t))^{p+1-k} \right) e^{-j\phi_{\mathrm{PN}}(t)} \\
& + \alpha_{\mathrm{R}} w(t) e^{j\phi_{\mathrm{PN}}} + \beta_{\mathrm{R}} w^{*}(t) e^{-j\phi_{\mathrm{PN}}}.
\end{aligned} \tag{3.37}
$$

After applying compensation algorithms, the residual values for remaining hardware impairments are usually small, so we limit ourselves to the most dominating effects. Considering this fact, in Paper C, we show that (3.37) for residual HWI can be approximated through statistical models, to a 1st-order accuracy, as

$$
\begin{aligned}
y_{\mathrm{R1}}(t) = \alpha_{\mathrm{T}}\alpha_{\mathrm{R}}\gamma_1\sigma_x \Bigg[& \underbrace{A\tilde{x}(t)}_{\text{useful signal}} + \underbrace{jA\sigma_{\phi}\Delta\tilde{\phi}(t)\tilde{x}(t)}_{\text{PN effect}} + \underbrace{A^{*}\left(\frac{\beta_{\mathrm{T}}}{\alpha_{\mathrm{T}}} + \frac{\alpha_{\mathrm{T}}^{*}\beta_{\mathrm{R}}\gamma_1^{*}}{\alpha_{\mathrm{T}}\alpha_{\mathrm{R}}\gamma_1}\right)\tilde{x}^{*}(t)}_{\text{IQI efect}} \\
& + \underbrace{A\left|\alpha_{\mathrm{T}}\right|^2 \frac{\gamma_3}{\gamma_1}\tilde{x}(t)\left|\tilde{x}(t)\right|^2\sigma_x^2}_{\text{PA nonlinearity effect}} + \underbrace{\frac{\sigma_{\mathrm{N}}}{\alpha_{\mathrm{T}}\gamma_1\sigma_x}\tilde{z}(t)}_{\text{noise}} \Bigg],
\end{aligned} \tag{3.38}
$$

where $y_{\mathrm{R1}}(t)$, is the first-order Taylor expansion of (3.37) by considering residual HWI effects. Equation (3.38) shows an additive and term-by-term description of how the signal of interest $x(t)$ is scrambled with different hardware impairment effects. In Paper C, we derive different orders of Taylor expansions of (3.37) to consider different levels of accuracy when we study the scrambled effects of HWI. We also show how additive noise modeling can be useful in distortion analysis and how it leads to accurate analysis of SDNR. In contrast to [25]–[37], our approach in Paper C can deliver more accurate term-by-term analysis of hardware impairments.

3.6 Antenna Array Perturbations

Antenna array perturbations play an important role in determining the overall performance of communication systems as they can result in deviations from desired beam direction and gain that can directly affect the array gain and capacity analysis. These perturbations, originating from the non-ideal physical characteristics of antenna arrays, primarily encompass phase and gain imbalances in antenna elements and element position perturbations.

Mathematical Model of Antenna Arrays

Let us contemplate a linear antenna array constituted by N elements arrayed along the z-axis, located at positions $\mathbf{p}_0, \mathbf{p}_1, ..., \mathbf{p}_{N-1}$, where the n-th position is represented as $\mathbf{p}_n = [0 \quad 0 \quad p_{n_z}]^T$. In line with Van Trees' definition [54], the array manifold vector can be portrayed mathematically as:

$$\mathbf{v}(\mathbf{k}) = \left[e^{-j\mathbf{k}\mathbf{p}_0} \quad e^{-j\mathbf{k}\mathbf{p}_1} \quad \dots \quad e^{-j\mathbf{k}\mathbf{p}_{N-1}}\right]^T. \tag{3.39}$$

Here, $\mathbf{k}$ denotes the wavenumber, capturing the direction of the array across any coordinate system. This wavenumber can be formulated as:

$$\mathbf{k} = \frac{2\pi}{\lambda}\left[\sin(\theta)\cos(\psi) \quad \sin(\theta)\sin(\psi) \quad \cos(\theta)\right], \tag{3.40}$$

where λ stands for the wavelength, θ signifies the angle directed towards the z-axis, and ψ is the angle offset from the x-axis. Then, the beam pattern is defined as [54]:

$$B(\theta, \psi) = B(\mathbf{k}) = \mathbf{w}^H \mathbf{v}(\mathbf{k}) = \sum_{i=0}^{N-1} g_i e^{j(\phi_i)} e^{-j\mathbf{k}\mathbf{p}_i}, \tag{3.41}$$

, where $\mathbf{w}$ is the complex gain vector with complex elements $w_i = g_i e^{j\phi_i}$. Here, each w_i is the complex gain of the i-th element in the phase shifter network (PSN), resulting from the operations of the vector modulator (VM), which incorporates a phase shifter and a variable gain amplifier (VGA).

Statistical Modeling of Array Perturbations

The perturbations in an antenna array can be understood as random fluctuations[1] impacting the parameters g_i, ϕ_i, and p_i in (3.41) as

$$B(\mathbf{k}) = \sum_{i=0}^{N-1} g_i(1 + \Delta g_i) e^{(j(\phi_i + \Delta\phi_i) - j\mathbf{k}\mathbf{p}_i)}, \tag{3.42}$$

with

$$\mathbf{p}_i = \mathbf{p}_i^c + [0 \;\; 0 \;\; \Delta p_i]^T, \tag{3.43}$$

where Δg, $\Delta\phi$, and Δp are defined as statistically independent, zero-mean, and Gaussian random variables and $\mathbf{p}_i^c$ is the vector of nominal element position in 3D space. These parameters can be determined based on the manufacturing process quality controls and for each of these parameters, a random variable with a predefined PDF based on empirical measurements can be assigned, where then the beam pattern can be represented as a random process over beam directions. In Paper D, we derive the higher-order statistics of the stochastic beam pattern function in (3.42). For the second-order statistics,

[1] These perturbations are modeled as random design parameters, not as random over time

we have:

$$
\begin{aligned}
\Lambda = & \sum_{i=0}^{N-1}\sum_{l=0}^{N-1}\sum_{m=0}^{N-1}\sum_{q=0}^{N-1} \\
& \Big[\Big(g_i g_l g_m g_q e^{j(\phi_i-\phi_l+\phi_m-\phi_q)} e^{-j\mathbf{k}(\mathbf{p}_i^c-\mathbf{p}_l^c+\mathbf{p}_m^c-\mathbf{p}_q^c)}\Big)\Big(1+(\delta_{mq}+\delta_{im}+\delta_{iq}+\delta_{lm}+\delta_{lq}+\delta_{il})\sigma_g^2 \\
& +(\delta_{il}\delta_{mq}+\delta_{im}\delta_{lq}+\delta_{iq}\delta_{lm})\sigma_g^4\Big)\Big(e^{\sigma_\phi^2(-2+(\delta_{mq}-\delta_{im}+\delta_{iq}+\delta_{lm}-\delta_{lq}+\delta_{il}))}\Big)\Big(e^{\sigma_\lambda^2(-2+(\delta_{mq}-\delta_{im}+\delta_{iq}+\delta_{lm}-\delta_{lq}+\delta_{il}))}\Big)\Big] \\
& -\Big(|B^c(\mathbf{k})|^2 e^{-(\sigma_\phi^2+\sigma_\lambda^2)} + [(1+\sigma_g^2)-e^{-(\sigma_\phi^2+\sigma_\lambda^2)}]\sum_{i=0}^{N-1} g_i^2\Big)^2
\end{aligned}
\tag{3.44}
$$

In paper D, we show that this model can statistically predict the random variation bounds on the beam pattern as depicted in Figure 3.3.

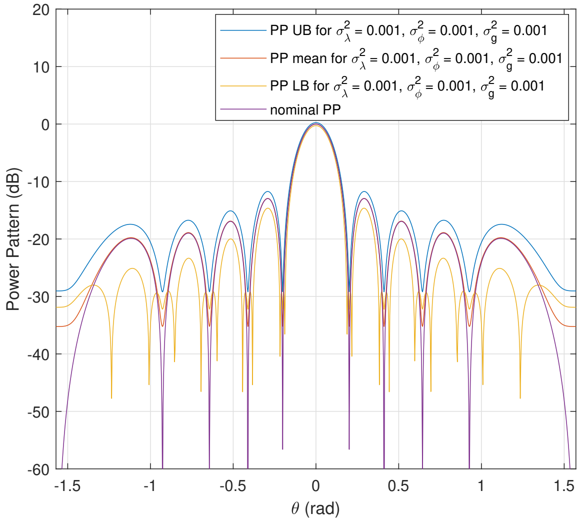

Figure 3.3: Beam pattern deviation bounds based on (3.44), **Paper D** ©2019 IEEE

CHAPTER 4

Summary of the Appended Papers, and Conclusion

In this section, we provide a summary of the four appended papers. For each paper, we have made a research question and then the summary of that paper is brought as the answer to that research question.

4.1 Paper A

M. H. Moghaddam, S. Rezaei Aghdam, N. Mazzali, and T. Eriksson, "Statistical Modeling and Analysis of Power Amplifier Nonlinearities in Communication Systems," *IEEE Trans. comm.*, Dec. 2021.

Research question 1: What is the scrambled effect of pulse shaping and matched-filter on PA nonlinearity effect in communication systems and how can we accurately formulate it?

Within the realm of communication systems and signal processing, pulse shaping and matched filtering constitute critical strategies for optimizing the transmission of signals. Nonetheless, these techniques may be substantially influenced by the nonlinear behavior of the power amplifier (PA), which could induce significant distortions in the signal and provoke inter-symbol interference. Such occurrences pose intricate challenges in ensuring dependable communication. The matched filtering procedure, employed for signal recovery at the receiver end, is similarly susceptible to the effects of PA nonlinearity. In Paper A, we undertake a comprehensive theoretical investigation into these impacts and subsequently corroborate our theoretical findings with empirical data from a real-world power amplifier.

4.2 Paper B

M. H. Moghaddam, K. Buisman, and T. Eriksson, "Theoretical Analysis of PA Nonlinearities,", to be submitted to *IEEE Commun. Lett.*

Research question 2: How does the effective PA nonlinearity manifest itself in distortion analysis? How does the distortion effect distribute in the in-band and out-of-band parts of the spectrum?

The effective nonlinearity of a PA refers to the mathematical representation of the nonlinearity present in the amplifier that leads to distortion. By analyzing the effective nonlinearity, researchers can gain insights into the characteristics of the distortion and develop techniques to mitigate its impact. Various mathematical models have been proposed to describe PA nonlinearity, such as the Volterra series, which allows the analysis of higher-order distortions. However, there is a gap in the literature when connecting the dots between input power, PA type, and input signal modulation type. Finding a descriptive model to fill this gap can help researchers explore methods to reduce distortions and improve the overall system performance. In paper B, we study this phenomenon and show that first, the third-order PA nonlinearity usually covers the most of distortion effect in comparison with higher-order distortions, and second, that the distortion can be represented as three factors related to signal power, amplifier coefficient, and a waveform factor.

4.3 Paper C

M. H. Moghaddam, S. Rezaei Aghdam, K. Buisman, and T. Eriksson, “Additive Noise Modeling: A Tractable Approach for Analyzing Residual RF Hardware Impairments,”, to be submitted to *IEEE Trans. Veh.*

Research question 3: What is the scrambled effect of residual hardware impairments in communication systems and how can we formulate them accurately?

The intricacies posed by PA nonlinearity in isolation are already substantial, but the situation becomes even more complex when this nonlinearity intersects with other hardware impairments, contributing further to the degradation of the communication system’s performance. Two such impairments of primary concern are IQI and phase noise. The combined influence of PA nonlinearity, IQI, and phase noise can generate a disruptive and scrambled effect, leading to a severe decline in the quality of the received signal. As we show in Paper C, an analytical study concerning this compounded effect proves to be of substantial importance, as it aids researchers in comprehending its impact on system performance and devising strategies to alleviate the collective influence of these impairments. We have also introduced additive noise modeling as a tractable technique for analyzing the scrambled effects of hardware impairments in communication systems. This method enables accurate tracking of system performance, considering not only individual hardware impairment parameters but also their collective interplay with other hardware impairments. By quantifying these influences, we can better comprehend the intricate dynamics at work, providing crucial insights that support the enhancement of system robustness amidst these perturbations.

4.4 Paper D

M. H. Moghaddam, S. R. Aghdam, and T. Eriksson, “Statistical Analysis of Antenna Array Systems with Perturbations in Phase, Gain and Element Positions.”, IEEE Global Conference on Signal and Information Processing, Ottawa, Ontario, Canada, Nov. 11-14, 2019.

Research question 4: How can array perturbations affect the final beam pattern? and how can we accurately formulate them to predict the beam variations?

In the context of Paper D, a robust analytical model is developed to investigate the impact of antenna array perturbations on the beam pattern of a linear antenna array. In particular, this model offers a comprehensive understanding of the statistical behavior of beam pattern perturbations caused by uncertainties in phase, gain, and antenna element position. The statistical formulation encapsulates the extent of these individual variations, allowing for a predictive approach toward understanding beam pattern fluctuations. In essence, the study offers a method by which the variations in the beam pattern can be accurately formulated as a function of the variance of each perturbing parameter. This approach, therefore, provides a more precise projection of system performance under diverse conditions, taking into account the inherent variability in the phase, gain, and position parameters of the antenna array.

4.5 Conclusion

This thesis has provided a comprehensive analysis of the impact of hardware impairments on communication systems, emphasizing the importance of understanding these effects. Through a detailed examination of PA nonlinearity, IQI, phase noise, and antenna array perturbations, the research has highlighted the significant role of statistical modeling of hardware impairments. The exploration of PA nonlinearity's effects, particularly in relation to pulse shaping, matched filtering, and transmitter-side distortions, has yielded crucial insights into how waveform characteristics, PA-specific parameters, and input signal power interplay to shape system behavior. The thesis has further advanced our understanding by proposing an additive noise model for analyzing the scrambled effects of PA nonlinearity, IQI, and phase noise, allowing for more accurate term-by-term distortion formulation. Additionally, the investigation into the impact of antenna array perturbations on beam patterns through first and second-order statistics offers valuable perspectives on manufacturing process variations. Overall, this work not only contributes to the field of communication systems engineering by providing a clearer picture of hardware impairment effects but also sets the stage for future research aimed at enhancing the reliability and efficiency of communication technologies.

References

[1] Worldometer. "Current world population." (), [Online]. Available: https://www.worldometers.info/world-population/.

[2] NASA. "Global climate change: Vital signs of the planet." (), [Online]. Available: https://climate.nasa.gov/vital-signs/carbon-dioxide/.

[3] U. N. E. P. N. K. Rep. "Un emissions gap report 2019." (), [Online]. Available: https://www.unep.org/resources/emissions-gap-report-2019.

[4] D. López-Pérez, A. De Domenico, N. Piovesan, *et al.*, "A survey on 5g radio access network energy efficiency: Massive mimo, lean carrier design, sleep modes, and machine learning," *IEEE Communications Surveys & Tutorials*, vol. 24, no. 1, pp. 653–697, 2022.

[5] GSMA. ""2019 mobile industry sdg impact report,"" (2019), [Online]. Available: https://www.gsma.com/betterfuture/2019sdgimpactreport.

[6] GSMA. "The enablement effect: The impact of mobile communications technologies on carbon emission reductions." (), [Online]. Available: https://www.gsma.com/betterfuture/enablement-effect.

[7] ITU. "Summary of smart 2020 report." (2020), [Online]. Available: https://www.itu.int/md/T05-FG.ICT-C-0004/en.

[8] ITU. "Sustainable ict in corporate organizations." (), [Online]. Available: https://www.itu.int/pub/T-TUT-ICT-2012-10.

[9] SMARTer2030. “Ict solutions for 21st century challenges.” (Feb. 2015), [Online]. Available: https://www.gesi.org/research/smarter2030-ict-solutions-for-21stcentury-%20challenges.

[10] L. Huawei Technologies Co. “Green 5g: Building a sustainable world.” (Feb. 2022), [Online]. Available: https://www.huawei.com/en/public-policy/green-%205g-building-a-sustainable-world.

[11] A. Abrol and R. K. Jha, “Power optimization in 5g networks: A step towards green communication,” *IEEE Access*, vol. 4, pp. 1355–1374, 2016.

[12] GSMA. “Going green: Benchmarking the energy efficiency of mobile.” (Jun, 2021), [Online]. Available: https://data.gsmaintelligence.com/research/research/%20research-2021/going-green-benchmarking-the-energy-efficiency-ofmobile.

[13] Vodafone. “2021 esg addendum.” (Jun, 2021), [Online]. Available: https://investors.%20vodafone.com/sites/vodafone-ir/files/2021-05/vodafone-esg-addendum-%202021.xlsx.

[14] M. Usama and M. Erol-Kantarci, “A survey on recent trends and open issues in energy efficiency of 5g,” *Sensors*, vol. 19, no. 14, p. 3126, 2019.

[15] J. Lorincz, A. Capone, and J. Wu, *Greener, energy-efficient and sustainable networks: State-of-the-art and new trends*, 2019.

[16] L. Pierucci, “The quality of experience perspective toward 5g technology,” *IEEE Wireless Communications*, vol. 22, no. 4, pp. 10–16, 2015.

[17] G. Auer, V. Giannini, C. Desset, *et al.*, “How much energy is needed to run a wireless network?” *IEEE wireless communications*, vol. 18, no. 5, pp. 40–49, 2011.

[18] G. Fettweis, M. Löhning, D. Petrovic, M. Windisch, P. Zillmann, and W. Rave, “Dirty rf: A new paradigm,” *International Journal of Wireless Information Networks*, vol. 14, no. 2, pp. 133–148, 2007.

[19] M. H. Moghaddam, S. R. Aghdam, A. Filippi, and T. Eriksson, “Statistical study of hardware impairments effect on mmwave 77 ghz fmcw automotive radar,” in *2020 IEEE Radar Conference (RadarConf20)*, IEEE, 2020, pp. 1–6.

[20] T. Schenk, *RF imperfections in high-rate wireless systems: impact and digital compensation.* Springer Science & Business Media, January 29, 2008.

[21] L. Ding, "Digital predistortion of power amplifiers for wireless applications," Ph.D. dissertation, Georgia Institute of Technology, 2004.

[22] G. Colavolpe, A. Barbieri, and G. Caire, "Algorithms for iterative decoding in the presence of strong phase noise," *IEEE J. Sel. Areas Commun.*, vol. 23, no. 9, pp. 1748–1757, Sept. 2005.

[23] U. Mengali, *Synchronization techniques for digital receivers.* Springer Science & Business Media, 2013.

[24] L. Anttila, M. Valkama, and M. Renfors, "Circularity-based I/Q imbalance compensation in wideband direct-conversion receivers," *IEEE Trans. Veh. Technol.*, vol. 57, no. 4, pp. 2099–2113, Jul. 2008.

[25] C. Studer, M. Wenk, and A. Burg, "Mimo transmission with residual transmit-rf impairments," in *2010 international ITG workshop on smart antennas (WSA)*, IEEE, 2010, pp. 189–196.

[26] E. Bjornson, P. Zetterberg, M. Bengtsson, and B. Ottersten, "Capacity limits and multiplexing gains of mimo channels with transceiver impairments," *IEEE Communications Letters*, vol. 17, no. 1, pp. 91–94, 2012.

[27] E. Björnson, J. Hoydis, M. Kountouris, and M. Debbah, "Massive mimo systems with non-ideal hardware: Energy efficiency, estimation, and capacity limits," *IEEE Transactions on information theory*, vol. 60, no. 11, pp. 7112–7139, 2014.

[28] J. Zhang, L. Dai, X. Zhang, E. Björnson, and Z. Wang, "Achievable rate of rician large-scale mimo channels with transceiver hardware impairments," *IEEE Transactions on Vehicular Technology*, vol. 65, no. 10, pp. 8800–8806, 2015.

[29] X. Zhang, M. Matthaiou, M. Coldrey, and E. Björnson, "Impact of residual transmit rf impairments on training-based mimo systems," *IEEE Transactions on Communications*, vol. 63, no. 8, pp. 2899–2911, 2015.

[30] A.-A. A. Boulogeorgos, N. D. Chatzidiamantis, G. K. Karagiannidis, and L. Georgiadis, "Energy detection under rf impairments for cognitive radio," in *2015 IEEE International Conference on Communication Workshop (ICCW)*, IEEE, 2015, pp. 955–960.

[31] X. Li, J. Li, Y. Liu, Z. Ding, and A. Nallanathan, "Residual transceiver hardware impairments on cooperative noma networks," *IEEE Transactions on Wireless Communications*, vol. 19, no. 1, pp. 680–695, 2019.

[32] T. T. Duy, T. Q. Duong, D. B. da Costa, V. N. Q. Bao, and M. Elkashlan, "Proactive relay selection with joint impact of hardware impairment and co-channel interference," *IEEE Transactions on Communications*, vol. 63, no. 5, pp. 1594–1606, 2015.

[33] H. Masoumi and M. J. Emadi, "Performance analysis of cell-free massive mimo system with limited fronthaul capacity and hardware impairments," *IEEE Transactions on Wireless Communications*, vol. 19, no. 2, pp. 1038–1053, 2019.

[34] J. Zhang, Y. Wei, E. Björnson, Y. Han, and S. Jin, "Performance analysis and power control of cell-free massive mimo systems with hardware impairments," *IEEE Access*, vol. 6, pp. 55 302–55 314, 2018.

[35] K. Guo and K. An, "On the performance of ris-assisted integrated satellite-uav-terrestrial networks with hardware impairments and interference," *IEEE Wireless Communications Letters*, vol. 11, no. 1, pp. 131–135, 2021.

[36] A. Papazafeiropoulos, E. Björnson, P. Kourtessis, S. Chatzinotas, and J. M. Senior, "Scalable cell-free massive mimo systems: Impact of hardware impairments," *IEEE Transactions on Vehicular Technology*, vol. 70, no. 10, pp. 9701–9715, 2021.

[37] A. Papazafeiropoulos, B. Clerckx, and T. Ratnarajah, "Rate-splitting to mitigate residual transceiver hardware impairments in massive mimo systems," *IEEE Transactions on Vehicular Technology*, vol. 66, no. 9, pp. 8196–8211, 2017.

[38] B. Razavi and R. Behzad, *RF microelectronics*. Prentice hall New York, 2012, vol. 2.

[39] A. Tarighat and A. H. Sayed, "Joint compensation of transmitter and receiver impairments in ofdm systems," *IEEE Transactions on Wireless Communications*, vol. 6, no. 1, pp. 240–247, 2007.

[40] P. Smulders, "Exploiting the 60 ghz band for local wireless multimedia access: Prospects and future directions," *IEEE communications magazine*, vol. 40, no. 1, pp. 140–147, 2002.

[41] J. J. Bussgang, "Crosscorrelation functions of amplitude-distorted Gaussian signals," Res. Lab. Elec., Cambridge, MA, USA, Tech. Rep. 216, Mar. 1952.

[42] S. C. Cripps *et al.*, *RF power amplifiers for wireless communications.* Artech house Norwood, MA, 2006, vol. 250.

[43] H. Ochiai, "An analysis of band-limited communication systems from amplifier efficiency and distortion perspective," *IEEE Transactions on Communications*, vol. 61, no. 4, pp. 1460–1472, 2013.

[44] S. Li and R. D. Murch, "An investigation into baseband techniques for single-channel full-duplex wireless communication systems," *IEEE Transactions on Wireless Communications*, vol. 13, no. 9, pp. 4794–4806, 2014.

[45] M. Schetzen, *The Volterra and Wiener theories of nonlinear systems.* Krieger Publishing Co., Inc., 2006.

[46] C. Mollén, U. Gustavsson, T. Eriksson, and E. G. Larsson, "Spatial characteristics of distortion radiated from antenna arrays with transceiver nonlinearities," *IEEE transactions on wireless communications*, vol. 17, no. 10, pp. 6663–6679, 2018.

[47] N. E. Cotter, "The stone-weierstrass theorem and its application to neural networks," *IEEE transactions on neural networks*, vol. 1, no. 4, pp. 290–295, 1990.

[48] F. H. Raab, P. Asbeck, S. Cripps, *et al.*, "Power amplifiers and transmitters for rf and microwave," *IEEE transactions on Microwave Theory and Techniques*, vol. 50, no. 3, pp. 814–826, 2002.

[49] S. Benedetto and E. Biglieri, *Principles of digital transmission: with wireless applications.* Springer Science & Business Media, 1999.

[50] E. Westesson and L. Sundstrom, "A complex polynomial predistorter chip in cmos for baseband or if linearization of rf power amplifiers," in *1999 IEEE International Symposium on Circuits and Systems (ISCAS)*, IEEE, vol. 1, 1999, pp. 206–209.

[51] K. Buisman, P. Landin, C. Fager, and T. Eriksson, *RFWebLab - Online RF Measurements*, `http://dpdcompetition.com/rfweblab/`, [Online; 2023], 2015.

[52] Ö. T. Demir and E. Björnson, "The bussgang decomposition of non-linear systems: Basic theory and mimo extensions," *arXiv:2005.01597*, 2020.

[53] A. Lahuerta, "Statistical modeling of non-linear amplifiers," 2016.

[54] H. L. Van Trees, *Optimum array processing: Part IV of detection, estimation, and modulation theory.* John Wiley & Sons, 2004.